2024 IEEE/ASME International Conference on Advanced Intelligent Mechatronics (AIM)
July 15-19, 2024. Boston, MA, USA

Soft Actuator Generating Various Torsional Motions Based on Helical Coupled Drive

Peizheng Yuan, Hideyuki Tsukagoshi*, *Member, IEEE*

***Abstract*—We present a soft pneumatic actuator that generates various torsional motions. Attempting to achieve this using conventional design methods resulted in an increase in the number of chambers and piping, which tended to narrow the range of motion. Therefore, we will introduce Helical Coupled Drive as a new design concept that generates a variety of curved shapes with as few chambers as possible. Namely, two helical actuators with variable pitch/phase/length are arranged in parallel so that they mechanically interfere with each other, and by adjusting their parameters. This drive method uses a total of six inputs, consisting of the air pressure of two chambers and the rotational angle of four motors, to create six representative types such as expansion-contraction / C-curve / J-curve / S-curve / helical / spiral. Furthermore, we also present a mechanical model and clarify the design parameters that define its shape. Finally, we verify the effectiveness of the proposed method by having the prototype grab a bottle and pour water into it.**

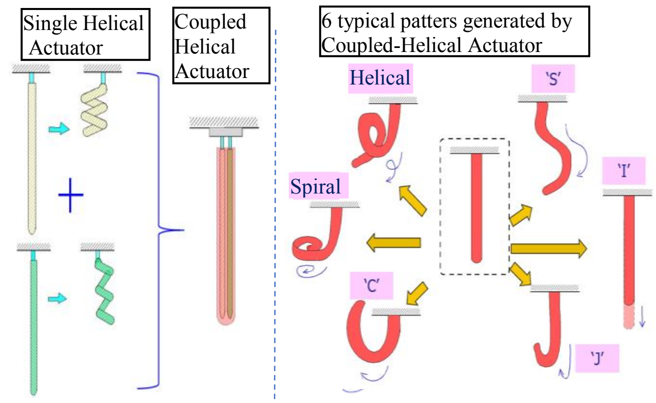

Figure 1. Concept of Helical Coupled Drive on left and motion patters generated by a Coupled-Helical Actuator based on the concept on right.

I. Introduction

Unlike traditional robots with rigid joints, Soft pneumatic actuators (SPAs) are primarily made of soft materials like rubber [1]-[2]. Because of their intrinsic dexterity and compliance, SPAs can achieve multiple degrees of freedom with a simpler structure compared to their rigid-body counterparts [3]. This makes them ideal for performing complex tasks in the real world, such as exploring complicated environments [4].

To achieve innovative kinematic mechanisms and large DOFs, many SPAs have been designed to mimic biological systems [5]. By drawing inspiration from animal, plants, insects, and other organisms, biomimetic SPAs with special hardware designs and actuation methods have been shown to be reliable for inspecting specific environments. For example, various inchworm-inspired SPAs have been applied in pipe inspection robots [6]-[8]. However, more complex deformations like turning require aligning several extensible SPAs in parallel [9] or using specific bending mechanisms [10]. Although bioinspired SPAs have been highly regarded for realizing specific application scenarios, the need for developing bio-inspired SPAs with multifunctionality remains urgent, given the complexity of exploring the real world [11].

To achieve multiple motion patterns, mimicking natural objects like an octopus arm or elephant trunk has become a popular approach in recent years [12]. The octopus arm and elephant trunk have similar anatomical structures, consisting entirely of soft tissue, with a central cord structure surrounded by transverse muscles and bundles of longitudinal muscle fibers arranged symmetrically [13]-[15].

Some researchers have attempted to simplify the structural complexity of the octopus arm and elephant trunk when building their SPAs. For instance, a soft robot arm, that used four controllable longitudinal fibers to mimic all the longitudinal muscles in the octopus arm, was developed [16]. Another study combined several cylindrical actuators serially with various functions, such as bending, twisting, contraction, and extension, to mimic the elephant trunk [17]. While these simplified structures may have small volumes, there would be a limit to realize the complex motions of the appendages they imitate.

In contrast, a robot arm with three bellows sets arranged in series [18] and the fruit harvesting manipulator [19], attempted to arrange a large number of contraction/extension actuators symmetrically to imitate the enormous muscle fibers in the elephant trunk, which resulted in the ability to realize complex motion patterns. On the other hand, in a configuration in which many soft pneumatic actuators are arranged in series as in the conventional method, the number of unpressurized chambers and pipes increases. As a result, the closer you get to the base, the more flexible movement is inhibited and the range of motion tends to decrease. This was the problem.

To fundamentally solve this problem, this research proposes a completely new drive method called Helical Coupled Drive (Fig.1). This method involves arranging multiple actuators that deform in a spiral shape in parallel and creating a variety of shapes through dynamic superposition. As a preparatory step, the authors proposed a method for designing and manufacturing a single helical actuator [20]. Furthermore, a four-input configuration was proposed, in which the inputs include two rotary actuators to change the phase in addition to the pressure of two chambers. However,

*Hideyuki Tsukagoshi is IEEE member and with Tokyo Institute of Technology, Japan. Peizheng Yuan was with Tokyo Institute of Technology.

with this configuration, only three patterns could be generated: C-curved/helical/spiral [21].

In this paper, in addition to the previous three patterns, we propose a new 6-input configuration that aims to generate J-shaped, S-shaped, linear stretch, and more diverse curved shapes. To achieve this, we will explain the basic concept of Helical Coupled Drive. Next, we will use illustrations to introduce specific drive configurations and motion patterns that can be generated. Then, we discuss a mechanical model to clarify the design parameters that define its shape. Finally, we verify the effectiveness of the proposed method by using the prototype device to grasp a plastic bottle and pour water into it.

II. Driving Principle

A. Coupled Helical Drive

Coupled Helical Drive, proposed in this paper, is a driving method in which multiple spiral-generating actuators are arranged in parallel (Fig.1). By making the pitch, phase, and length of each actuator variable, it is expected that they will mechanically interfere with each other and produce a variety of shapes.

The elements that realize this drive are multiple flexible chambers that transform from a linear shape to a spiral shape when pressurized, actuators such as motors that change pitch, phase, length, etc., and anisotropic stretch fabric. The anisotropic stretch fabric is a flexible fabric that is easy to stretch in the axial direction and difficult to stretch in the radial direction. Cover the chamber from the outside. Additionally, the chamber is restrained at its ends so that it can rotate.

Specifically, we will introduce the configuration shown in Fig.2. Two motors for rotation (a1, a2) and two motors for changing the length of the restraint string (b1, b2) are installed at the top. The phase is adjusted by the rotation angle of the rotation motor. The length is adjusted by a restraining thread motor. The pitch can be changed by pressure in addition to the rotation angle of the rotation motor and the length adjustment motor.

The primitive coupled helical actuator proposed in the paper [21] had only four inputs, so the phase and pitch couldn't to be adjusted independently. Therefore, only three patterns were generated: C-shaped curve, helical, and spiral which curls in plane. Since the actuator proposed in this study has six inputs, the phase, pitch, and length can be changed independently, so it is expected that six types of shapes can be realized.

B. Motion patterns

A couple helical actuator with 6 inputs, which we call SEMI-TRUNK, can generate different motion patterns as follows.

When motors b1 and b2 are rotated in opposite directions so that the thread lengths increase by l on both sides. When the same pressure p is applied in both tubes, they perform linear extension from their initial length L_0 to L, the length after being pressurized, with L satisfying the following relationship:

$$L < L_0 + l. \tag{1}$$

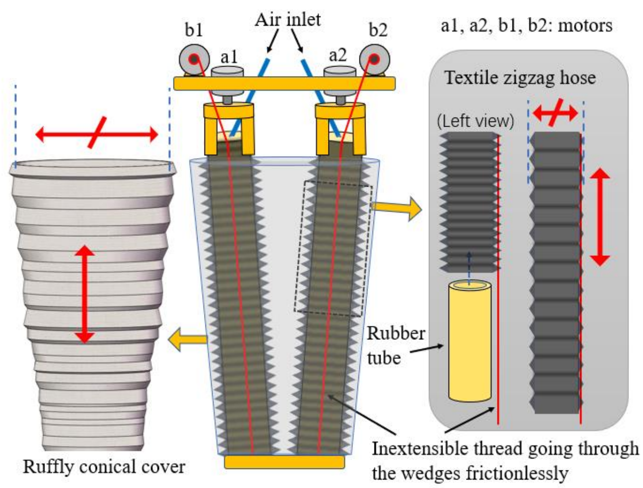

Figure 2. Driving mechanism of SEMI-TRUNK with 6 inputs

Then, let us consider another situation. Suppose we keep the initial thread length L_0 and apply the same pressure p in both tubes. In this case, not only the radial expansions of two tubes are blocked by the hose, the longitudinal extension on the front sides of the tubes are also restricted by the two threads. Thereby, the SEMI-TRUNK bends towards the top front, like a letter "C" in a vertical plane, as shown in the 3rd column of Fig. 3.

To realize J-shaped bending, we first control motors a1 and a2 to rotate the top parts of the tubes 90° in opposite directions. We define this rotation angle as the top twisting angle θ, which is positive when the tube is rotated to the left and negative to the right. In the following context, θ of the left tube is denoted as θ_1 and θ of the right tube is denoted as θ_2. In this case, θ_1 equals -90° and θ_2 equals 90°. The inextensible threads of the SEMI-TRUNK start from the front edges at the bottom and extend to the left and right edges at the top of the tubes.

Naturally, when the same pressure p is applied in each tube, the tube tends to curve along the inextensible thread. Because the thread is twisted along the tube, if we decompose the curving force on every sectional plane along one tube, we can see that as the sectional plane shifts from the bottom to the top, the forward component of the curving force decreases from the maximum to 0; meanwhile the transverse component of the curving force increases from 0 to the maximum, as shown in the 4th column of Fig. 3.

At the same time, due to the existence of the ruffly conical cover (an anisotropic stretch fabric), the leftward force component in the left tube and the rightward force component in the right tube always cancel each other out in the horizontal direction; then, only the forward curving forces remain and result in two-dimensional bending, with the curvature decreasing from the tip to the top of the actuator. When observed from the right side, this deformation is like a letter "J." Thus, we call this the J-shaped bending.

Based on the above analysis, we can also notice that if the top twisting angle θ is larger than 90° (or less than -90°), top parts of the thread tend to twist to the back semi-circle of the tube so that this part of the actuator will generate a backward

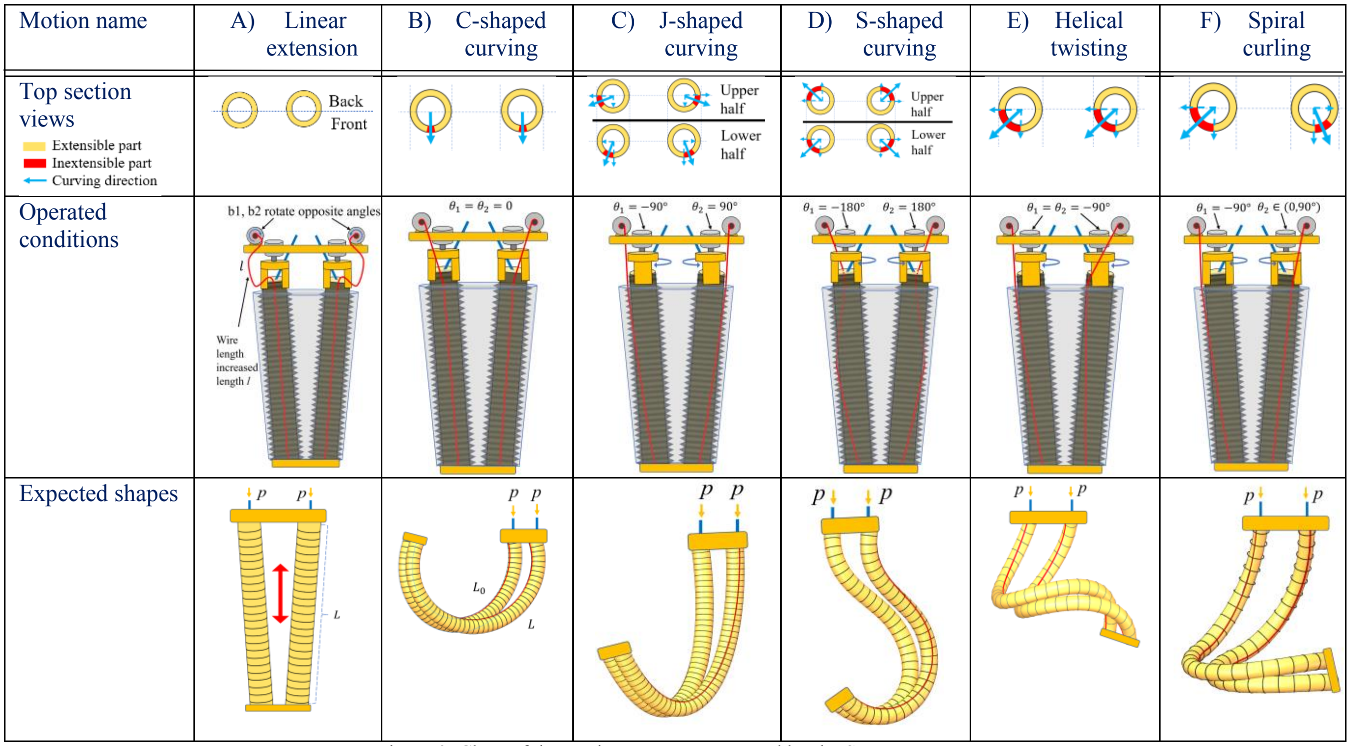

Figure 3. Chart of the motion patterns generated by the SEMI-TRUNK.

curving force after being pressurized. For instance, let us consider the situation when we twist the left tube -180° and the right tube 180° and then pressurize them with the same pressure *p*. Naturally, the threads in the lower half remain forward while in the top half, the threads turn backward. Therefore, in the lower half part of the SEMI-TRUNK, symmetric curving forces point to the right-front and left-front, and in the upper half part of the COMBINED-HELICAL, a symmetric right-backward curving force and left-backward curving force exist. Like the J-shaped bending, all the symmetric transverse force components cancel each other out, and only the forward curving components in the lower half and the backward curving components in the upper half remain. The SEMI-TRUNK performs S-shaped bending, as shown in the 5th column of Fig. 3

To realize 2D deformation, we rotate two tubes towards opposite directions with the same angles. In contrast, to realize 3D deformation, an asymmetric structure is used.

Let us consider the situation when both tubes are rotated by the same angle to the left, with θ_1 and θ_2 equaling -90° for example, and then pressurized. Because the curving directions in the two tubes are identical, they do not cancel out but enhance each other. The whole actuator curves along the inextensible thread and makes a helical bending with the influence of gravity. When θ is negative, the SEMI-TRUNK makes a counter-clockwise helix, and with a positive θ, the SEMI-TRUNK makes clockwise helix (top view), as shown in the 6th column of Fig. 3.

Spiral bending can be realized when the left tube is rotated -90° while the right tube is rotated with a positive angle less than 90° (typically 0-40°), with the same pressure applied. The two tubes tend to twist in opposite directions, but because the left tube generates a larger transverse curving component, the SEMI-TRUNK twists in a counter-clockwise direction. With the resistance force of the right tube, the curvature in the upper part of the SEMI-TRUNK is less than that of the helical bending when θ_1 and θ_2 equal -90°. In the lower part, the forward curving components get larger; meanwhile, the transverse components get smaller, considering the influence of gravity, and both tubes tend to curve towards the same direction, generally inside a 2D plane, as shown in the 7th column of Fig. 3.

In the 2nd row of Fig. 3, the top section views show the extensible and inextensible parts along the directions of the curving forces in two tubes. The 3rd row shows how the top twisting angles are changed and the corresponding twisted sub-actuators. In the final row, the expected deformations are shown after the SEMI-TRUNK is pressurized, where the black rings represent the transverse restrictions of the zigzag hoses and the red line represents the inextensible threads.

Note that there are many possible shapes in the spiral bending motion, and Fig. 3 only shows one pose of this motion pattern. An obvious factor that can largely enrich the deformation shapes is the inextensible thread length L_0. When a constant pressure is maintained, increasing or decreasing the threads' lengths together can change the curvatures in the "C," "J," and "S" deformations, but it cannot only change the height of the tip point while keeping the whole stiffness of the actuator in these deformations. In addition, applying different thread lengths in the helical or spiral deformation can largely increase the complexity with adjustable θ or p at the same time.

III. Modeling

This chapter describes the models to quantitatively demonstrate the deformation processes of different motion patterns of the SEMI-TRUNK. Because spiral bending has too many possible shapes, this motion pattern was not modeled.

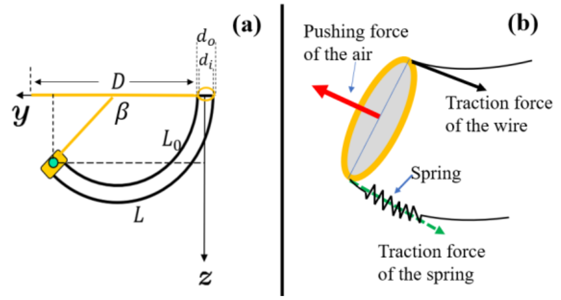

Figure 4. Simplified mechanical model of curving shown in SEMI-TRUNK

For the other motion patterns, mathematical models were established for the linear extension motion and the C-shaped bending motion. Simulation models were built for the C-shaped bending, J-shaped bending, S-shaped bending, and helical bending motions to reveal their morphological changes and the displacements of the tip point of the actuator under different pressures. Because the SEMI-TRUNK is designed to have a much larger length than its width to imitate the elephant trunk, we regard elongation of the SEMI-TRUNK as the same as the elongation of the sub-actuators in our modeling.

In the linear extension, after the two sub-actuators are pressurized with the same pressure p, considering the force balance at the bottom connector, we have

$$mg + 2p\frac{\pi d_i^2}{4} = 2EA\frac{L - L_0}{L_0}, \tag{2}$$

where m is the mass of the actuation part of the SEMI-TRUNK without the motor frame, g is the gravitational acceleration, d_i is the inner diameter of the rubber tube, E is the Young's modulus of the tube, and A is the sectional area of the tube, which we assume as constant during the deformation. L is the current length of the actuator after pressurization, and the length A can be calculated using the following equation:

$$A = \frac{\pi(d_o^2 - d_i^2)}{4}, \tag{3}$$

where d_o is the outer diameter of the tube. Using (2) and (3), we obtain the relationship between the pressurized actuator length and the input pressure as follows:

$$L = (\frac{2mg + p\pi d_i^2}{E\pi(d_o^2 - d_i^2)} + 1)L_0. \tag{4}$$

For the C-shaped bending, we ignore the influence of gravity, and thus the deformed shape of the actuator can be regarded as an arc with inner diameter D and center angle β inside a plane, as shown in Fig. 4(a).

We build an x-y-z coordinate system with the origin set at the center of the bottom plane of the motor frame. Observed from the front, the x-axis points rightward, the y-axis points forward, and the z-axis points downward, as shown in Fig. 4(a). Because the whole actuator and inputs are symmetric about the *y-z* plane, we can analyze just one sub-actuator. We also regard the traction force of the whole rubber tube as a spring that lies along the outer edge of the tube, and assume the traction force of the spring after extension follows Hooke's law, as shown in Fig. 4(b).

In this case, if we consider the torque balance and force balance at the tip of each sub-actuator formed by the pushing force of the inside air, the traction forces of the spring and the thread shown in Fig. 4(b), we have

$$p\frac{\pi d_i^2}{4} = T + k\left(L - L_0\right), \tag{5}$$

$$T\frac{d_o}{2} - k(L - L_0)\frac{d_0}{2} = 0, \tag{6}$$

where T is the traction force of the thread, k is the spring constant, and L is current length of the outer edge of the curved tube. From (5) and (6), we have

$$L - L_0 = p\frac{\pi d_i^2}{8k}. \tag{7}$$

From Fig. 4(a), we have

$$L - L_0 = \beta(\frac{D}{2} + d_o) - \beta\frac{D}{2} = \beta d_o. \tag{8}$$

Using (7) and (8), we obtain

$$\beta = \frac{p\pi d_i^2}{8kd_o}, \tag{9}$$

and thus,

$$D = \frac{2L_0}{\beta} = \frac{16kd_oL_0}{p\pi d_i^2}. \tag{10}$$

We can see that with L_0 settled, β has a proportional relationship with the input pressure p; meanwhile, D has an inverse proportional relationship with p.

If we define the coordinates of the center part of the tip as *(x, y, z)*, we have

$$x = 0, y = \frac{D + d_o}{2}(1 - \cos\beta), z = \frac{D + d_o}{2}\sin\beta. \tag{11}$$

Based on (9), (10), and (11), the coordinate changes of the tip of the SEMI-TRUNK during the C-shaped bending motion can be represented by the following equation with an unknown coefficient k:

$$\begin{aligned} & x = 0, \\ & y = f_1(k,p) = (\frac{8kd_oL_0}{p\pi d_i^2} + \frac{d_o}{2})(1 - \cos\frac{p\pi d_i^2}{8kd_o}), \\ & z = f_2(k,p) = (\frac{8kd_oL_0}{p\pi d_i^2} + \frac{d_o}{2})\sin\frac{p\pi d_i^2}{8kd_o}. \end{aligned} \tag{12}$$

The y and z coordinates are both functions of k and p. The best value of k in the model can be easily chosen through least squares fitting with several pairs of experimental data under the same pressures. The fitting process is described in section V.

IV. Experiments

This section explains how we designed and conducted experiments to evaluate the effectiveness of our mathematical models.

A. *Developed mechanical model*

We first inserted the two tubes into the zigzag hoses, sewed the threads through the wedges of corresponding hoses, and then connected them using the bottom connector. In this way, two sub-actuators were prepared as shown in Fig. 6(c). To decrease the friction between the thread and the hose, we passed the threads through the wedges once every four wedges.

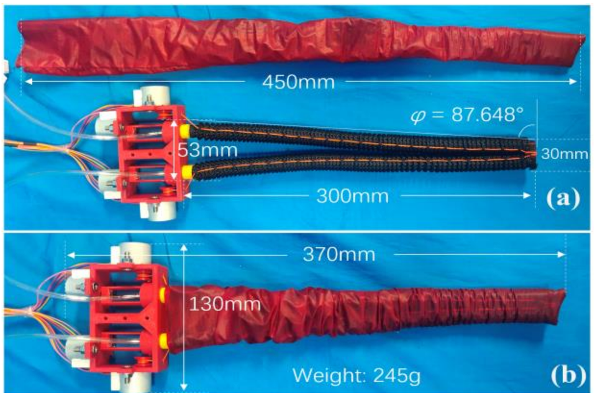

Figure 5. Overall view of developed SEMI-TRUNK

The top parts of the sub-actuators were connected to a 3D-printed motor frame, whose structure is shown in Fig. 5. The

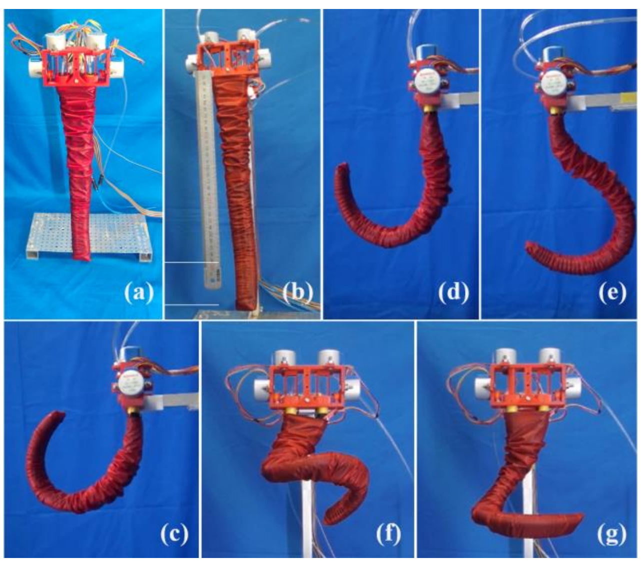

Figure 6. 6 typical motion patterns generated SEMI-TRUNK, which can be also observed in an actual elephant's trunk

two tubes were connected to two stepper motors through vertical rotational shafts with a 38 mm center-to-center distance. The inextensible threads were connected to two other stepper motors by pulleys so that when the motors produced rotation, the lengths of the inextensible threads could be adjusted. The stepper motors we used were 24BYJ-48, which could generate pull-in torque larger than 29.4 mN·m. We used the ULN2003 motor driver to drive them under 12 V DC, and all four motors were controlled using an Arduino Mega 2560 controller.

After the sub-actuators were connected to the motor frame, the main part of the SEMI-TRUNK was finished as shown in Fig. 6. The length of the actuation part was kept at 300 mm. The upper width of the actuation part was 53 mm, and the lower width was 30 mm. The dip angle of the sub-actuator φ, which is the closed angle between the sub-actuator and the bottom, was 87°.

Fig. 5 shows the size of the SEMI-TRUNK with the conical cover. The prototype was 370 mm long and weighed 245 g, but its actuation part only weighed 78 g. Its widest part reached 120 mm, and its narrowest part was only 30 mm wide.

B. *Followability*

For the linear extension motion, we used a ruler to measure the length change of the SEMI-TRUNK under linearly increased pressure from 0 to 0.2 MPa and then compared the result with that of the mathematical calculation using (4). The comparison results are shown in Fig. 7.

Judged from them, we can conclude that the mathematical model generally fits the experiment results with the prototype. We noticed that the initial lengths of the model and the prototype have almost the same value, while as the pressure increases, the actual length of the actuator remains smaller than the modeling result. We believe this error is due to the friction inside the prototype (rubber tubes and the zigzag hoses for instance), which we did not include in our model.

For the other four motion patterns, we used the experimental device shown in Fig. 7 to measure and record the coordinate changes of the tip of the SEMI-TRUNK. As the figure shows, a yellow marker was attached to the tip of the SEMI-TRUNK. On the right side of the actuator was a depth camera, an Intel Realsense D435. Possessing two parallelly arranged infrared cameras, the D435 can calculate the depth distance of any point inside its frame based on the differences of the pixel coordinates of the two cameras. The measurement error of the camera reaches 2% in the range from 0.2 m to 2 m.

As shown in Fig. 7(a), two coordinate systems were set. We defined the world coordinate system x-y-z with the origin

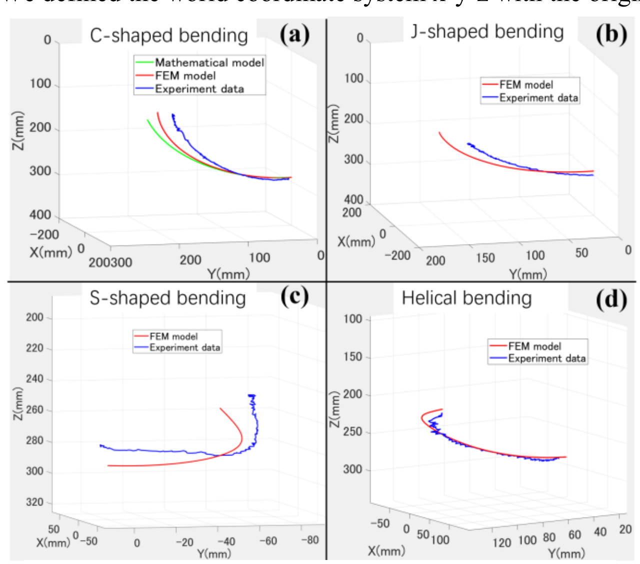

Figure 7. Comparison of the trajectory of the tip derived from the mathematical model and the trajectory of the tip of the prototype

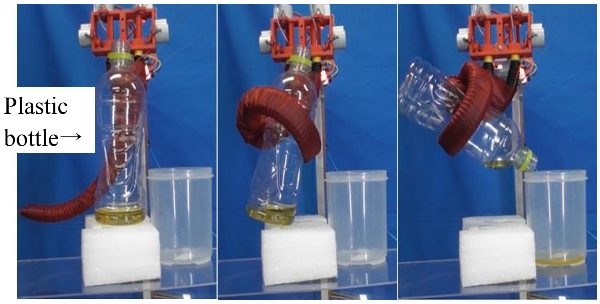

Figure 8. Operation of grasping a plastic bottle and pouring water by combing Helical and Spiral shape motions

set at the bottom center of the motor frame. The x-axis points right, the y-axis points forward, and the z-axis points downward. The origin of the camera coordinate system $x'-y'-z'$ lies at the inferred center point of two cameras, together with a backward x-axis, downward y-axis, and leftward z-axis.

As the experiments began, we increased the air pressure in the two sub-actuators of SEMI-TRUNK simultaneously and linearly from 0 to 0.2 MPa, as in the FEM simulations. As Fig. 9(b) shows, the coordinates of the tip of the actuator in the camera coordinate system were printed on the captured frame and recorded. The video stream consisted of 30 frames per second with 640×480 pixels in each frame. After that, we designed a Gaussian filter to suppress the measurement error in the recorded data and then transform them into the coordinates in the world coordinate system.

C. *Manipulation of a plastic bottle*

As shown in Fig. 8, a small plastic bottle of green tea and a cup were placed on a platform. The cylindrical bottle was 205 mm high, and its maximum diameter was 65 mm. The bottle weighed 18 g and the tea inside it weighed 42 g. Our target in this scenario was to control the SEMI-TRUNK to first grab this bottle of green tea, lift it up, and then pour it into a nearby cup. We chose this scenario because fetching a cup of tea satisfies the general expectation of what a practical robot arm should be able to do to assist humans in the real world.

The maximum payload of this scenario was about 68 g under 0.2 MPa, but this was slightly influenced by the thread length during the grabbing and transferring process. All the control signals were manually given from a laptop to the Arduino controller through a serial port to make the actuation speed adjustable.

V. Conclusion

In this paper, we introduced a new pneumatic soft actuator that could perform diverse bending and extension motions based on a new design concept called Coupled Helical Drive. By combining two helical shapes whose phase, pitch, and length could be adjusted independently, we showed that various motions, including six representative shapes, could be realized. Compared to the four-input case where the phase and pitch are adjusted dependently as shown in the previous paper, we confirmed that it is possible to generate many more shape patterns. In addition, we established a mathematical model to predict changes in the tip position during various deformations, and the prototype device “SEMI-TRUNK" operated as intended and was able to grasp a plastic bottle and pour tea into a cup. As a future project, we plan to establish an inverse kinematics model in order to control the shape while supporting a load.

References

[1] S. M. Xavier, et al, “Soft pneumatic actuators: A review of design, fabrication, modeling, sensing, control and applications,” in *IEEE Access*, vol. 10, no. 1, 2022, pp. 59442-59485.

[2] J. Walker, et al, “Soft robotics: A review of recent developments of pneumatic soft actuators,” in Actuators, vol. 9, no. 1,2020, pp. 3-30.

[3] D. Rus, M. T. Tolley, “Design fabrication and control of soft robots,” in *Nature*, vol. 521, 2015, pp. 467-475.

[4] C. Laschi, B. Mazzolai, M. Cianchetti, “Soft robotics: Technologies and systems pushing the boundaries of robot abilities,” in *Science Robotics*, vol. 1, no. 1, 2016, eaah3690.

[5] J. Wang, et al, “A survey of the development of biomimetic intelligence and robotics,” in *Biomimetic Intelligence and Robotics*, vol. 1, 2021, pp. 100001.

[6] A. Verma, et al, “A review on various types of in-pipe inspection robot,” in *Materials Today: Proceedings*, vol. 50, no. 5, 2021, pp. 1425-1434.

[7] R. Ab, Z. Mohd, et al, “Modeling of the in-pipe inspection robot: A comprehensive review,” in *Ocean Engineering*, vol. 203, 2020, pp. 107206.

[8] K. Miyasaka, G. Kawano, H. Tsukagoshi, “Long-mover: Flexible tube in-pipe inspection robot for long distance and complex piping,” in *2018 IEEE/ASME International Conference on Advanced Intelligent Mechatronics (AIM)*, IEEE, 2018, pp. 1075-1080.

[9] Z. Zhang, et al, “Design and modeling of a parallel-pipe-crawling pneumatic soft robot,” in *IEEE access*, nol. 7, 2019, pp. 134301-134317.

[10] B. Zhang, et al, “Worm-like soft robot for complicated tubular environments,” in *Soft robotics*, vol. 6, no. 3, 2019, pp. 399-413.

[11] M. Ilami, et al, “Materials, actuators, and sensors for soft bioinspired robots,” in *Advanced Materials*, vol. 33, no. 19, 2021, pp. 2003139.

[12] A. Das, M. Nabi, “A review on soft robotics: modeling, control and applications in human-robot interaction,” in *2019 International Conference on Computing, Communication, and Intelligent Systems (ICCCIS)*, IEEE, 2019, pp.306-311.

[13] E. B. Kennedy, et al, “Octopus arms exhibit exceptional flexibility,” in *Scientific reports*, vol.10, no.1, 2020, pp. 1-10.

[14] P. Dagenais, et al, “Elephants evolved strategies reducing the biomechanical complexity of their trunk,” in *Current Biology*, vol. 31, no.21, 2021, pp. 4727-4737.

[15] K. A. Schulz, et al, “Skin wrinkles and folds enable asymmetric stretch in the elephant trunk,” in *Proceedings of the National Academy of Sciences*, vol. 119, no. 31, 2022, e122563119.

[16] C. Laschi, et al, “Soft robot arm inspired by the octopus,” in *Advanced robotics*, vol. 26, no. 7, 2012, pp. 709-727.

[17] Q. Guan, et al, “Novel bending and helical extensile/contractile pneumatic artificial muscles inspired by elephant trunk,” in *Soft robotics*, vol. 7, no. 5, 2020, pp. 597-614.

[18] [online] Available: https://www.festo.com/us/en/e/about-festo/research-and-development/bionic-learning-network/highlights-from-2015-to-2017/bionicsoftarm-id_68209/.

[19] T. Shao, et al, “Fruit harvesting continuum manipulator inspired by elephant trunk,” in *International Journal of Agricultural and Biological Engineering*, vol. 8, no.1, 2015, pp. 57-63.

[20] P. Yuan, G. Kawano, H. Tsukagoshi, “Soft Pneumatic Helical Actuator with High Contraction Ratio,” in 2019 *IEEE/RSJ International Conference on Intelligent Robots and Systems (IROS)*, IEEE, 2019, pp. 8300-8305.

[21] P. Yuan, H. Tsukagoshi, “Double Helical Soft Pneumatic Actuator Capable of Generating Complex 3D Torsional Motions,” in *IEEE Robotics and Automation Letters*, vol. 6, no. 4, 2021, pp. 8142-8149.